# 28

# Fluvial Gravels on Mars: Analysis and Implications

*William E. Dietrich, Marisa C. Palucis, Rebecca M. E. Williams, Kevin W. Lewis, Frances Rivera-Hernandez, and Dawn Y. Sumner*

## 28.1 Introduction

Decades of satellite imagery of Mars have provided strong evidence of an extensive early history of fluvial processes (e.g. Carr and Clow 1981; Craddock and Howard 2002; Moore *et al.* 2003; Malin and Edgett 2003; Moore and Howard 2005; Irwin *et al.* 2008). Channel networks, giant outflow channels, meandering channels, deltas, and fans have been mapped across the planet, and the relative timing of fluvial erosion and deposition events has been estimated from the number and size of craters found on mapped units (e.g. Irwin *et al.* 2008; Carr 2012). These features make a strong case that the early Mars climate had an atmosphere capable of producing precipitation and lasting long enough for a sustained hydrologic cycle. The last period of widespread and extensive fluvial activity ended about 3.5 billions of years ago (e.g. Fassett and Head 2008), and yet while this is still fairly early in Mars' history, climate models suggest that a sustained atmosphere at this time was unlikely, and it remains difficult to predict for even wetter, earlier periods (e.g. Woodsworth *et al.* 2013; Carter *et al.* 2015). This interpretation, in part, has led to a reassessment of fluvial features. Some have proposed, based on modeling, that fans and deltas could form in just a few years, and thus might be the product of transient precipitation from a major impact (e.g. Kleinhans 2005; Kleinhans, van de Kasteele, and Hauber 2010; Mangold *et al.* 2012). Others have considered the possibility that features that appear to be of fluvial origin, may be gas driven, due to eruptive volcanism, or other processes involving little or no running water (e.g. Gulick 1998; Gulick and Baker 1990).

For the first time, as a result of the Mars Science Laboratory (MSL) mission and photographs obtained by the *Curiosity* rover, fluvial gravels have been directly observed on Mars. These observations strongly support previous satellite-based interpretations that fluvial processes have been active on Mars. They also allow us to examine shape, sorting, and grain size. Here we first describe initial observations and interpretations of Martian fluvial gravels. We then show some examples of exposed conglomerates that the rover has crossed during its first 10 km of travel. These observations present a fundamental challenge of great interest on Mars: how much paleohydrologic and climatic information can we extract from a gravel deposit. We review two approaches to reconstructing instantaneous flows and explore the problem of estimating flow when only the grain-size distribution is known. Finally, we

*Gravel-Bed Rivers: Processes and Disasters*, First Edition. Edited by Daizo Tsutsumi and Jonathan B. Laronne.

show how the total volume of sediment in a deposit (e.g. alluvial fan) has been used to estimate the runoff volume and thus place constraints on the climate history of Mars.

## 28.2 First Observations of Fluvial Conglomerates on Mars

*Curiosity* landed on Mars on August 6, 2012 (UTC) on the northern floor of Gale Crater (5.3°S 137.7°E), an impact structure that formed about 3.8–3.6 billion years ago (Thompson *et al.* 2011; Le Deit *et al.* 2013; Figure 28.1). This 157 km diameter crater has a 5 km central mountain of sedimentary rocks (Aeolis Mons) that towers by 2 km over the northern rim of the crater. Remarkably, it was the scour caused by the thrust from the descent engines during *Curiosity's* landing that revealed a lithified, almost concrete-like, appearance to the underlying deposit at the landing site. The exposure at the landing site and subsequently outcrops found in the initial traverse by the rover to the northeast are described in Williams *et al.* (2013) (Figure 28.2). The initial debate upon observing these deposits was about the transport mechanism, which is particularly significant in regards to the volume of water and hence climatic conditions during transport and deposition. Did these deposits record fluvial transport as bedload and suspended load or could these deposits record debris-flow processes (and consequently much less water involved)? Questions were initially raised as well as to whether the deposits did in fact record water-driven transport processes. The key properties of these deposits (Figure 28.2) are: (i) distinctly well-rounded shapes; (ii) local sorting such that like-sized particles were co-deposited; (iii) vertical variation in sorting (stratification); (iv) grain to grain contact (i.e. not matrix supported); (v) some locations of grain imbrication; and (vi) particle sizes up to 40 mm in diameter. Collectively, these properties strongly indicate fluvial transport. Perhaps most persuasive is the strong rounding of particles that are too large to be transported by wind. Not only does this suggest a collisional transport process (i.e. bedload transport) but also a travel distance, which Williams *et al.* (2013) suggest was at least a few kilometers. The median grain size from three outcrops found near the landing site ranged from 4.5 to 9.5 mm. Yingst *et al.* (2014) also found rounded pebbles lying on the surface at various locations over a distance of about 400 m from the initial landing site.

No sense of scale of the fluvial system was indicated in the outcrops; that is, we did not see channel-scale bedding features or preserved banks. These first observations were made in an elevated area (referred to as Bradbury Rise) within a closed basin that lies between Mt Sharp (Aeolis Mons) and the crater wall and into which the terminal end of the Peace Vallis fan enters (Figures 28.1c and 28.3). The Rise is on the shoulder of a ridge that connects the base of Mount Sharp to the crater wall. As Palucis *et al.* (2014) illustrate, this Rise lies downslope of the Peace Vallis fan (Figure 28.3) and it is possible that sheetfloods from the Peace Vallis fan swept across this area (see figure 15 in Palucis *et al.* 2014). Local topography, however, indicates that wind deflation has occurred, and the deposits may thus be exhumed and hence record an earlier period of deposition, perhaps associated with the processes that formed the ridge that crosses the crater floor. Malin and Edgett (2000) proposed that Gale was once entirely filled with sediment and then subsequently a ring of scour developed (presumably by wind deflation) that left a towering (~5 km) low-gradient mountain in the center of the crater in which remnants of the prior deposits are exposed (Figure 28.1). If this occurred, Palucis *et al.* (2014) argue that the Peace Vallis fan developed after the crater was subsequently exhumed. The origin of Mount Sharp sediments awaits direct observations by *Curiosity* of the basal sediments (Grotzinger *et al.* 2015)

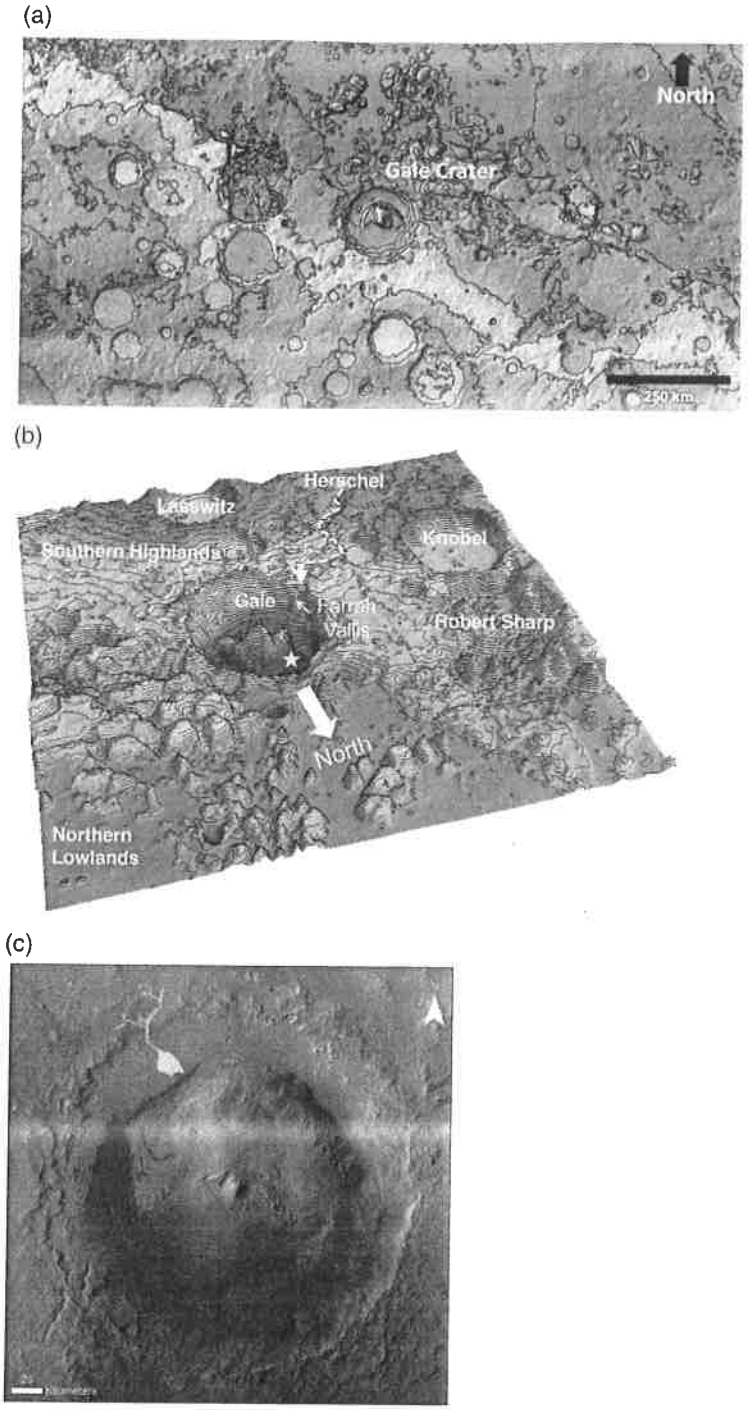


**Figure 28.1** (a) Shaded relief map (with 1000 m contours) of Gale Crater and the surrounding region generated from MOLA (Mars Orbiter Laser Altimeter) data. Gale Crater is located on the crustal dichotomy between the cratered southern highlands and the smoother northern lowlands of Elysium Planitia. (b) A closer view of Gale Crater and its surrounding terrain. The lowest elevations in Gale Crater occur on the northwest portion of the crater floor, near the MSL landing site. Gale's impact disrupted a pre-existing valley network originating near Herschel Crater; this was likely one of the main early sources of water into Gale Crater. (Based on Irwin *et al.* (2005).) (c) Mosaic of satellite photographs of Gale Crater derived from Mars Reconnaissance Orbiter Context Camera CTX. Peace Vallis fan and the upstream incised channel network that provided sediment to the fan are shown in a light tone. The star is the *Curiosity* rover landing site. (See insert for color representation of Figure 28.1b.)

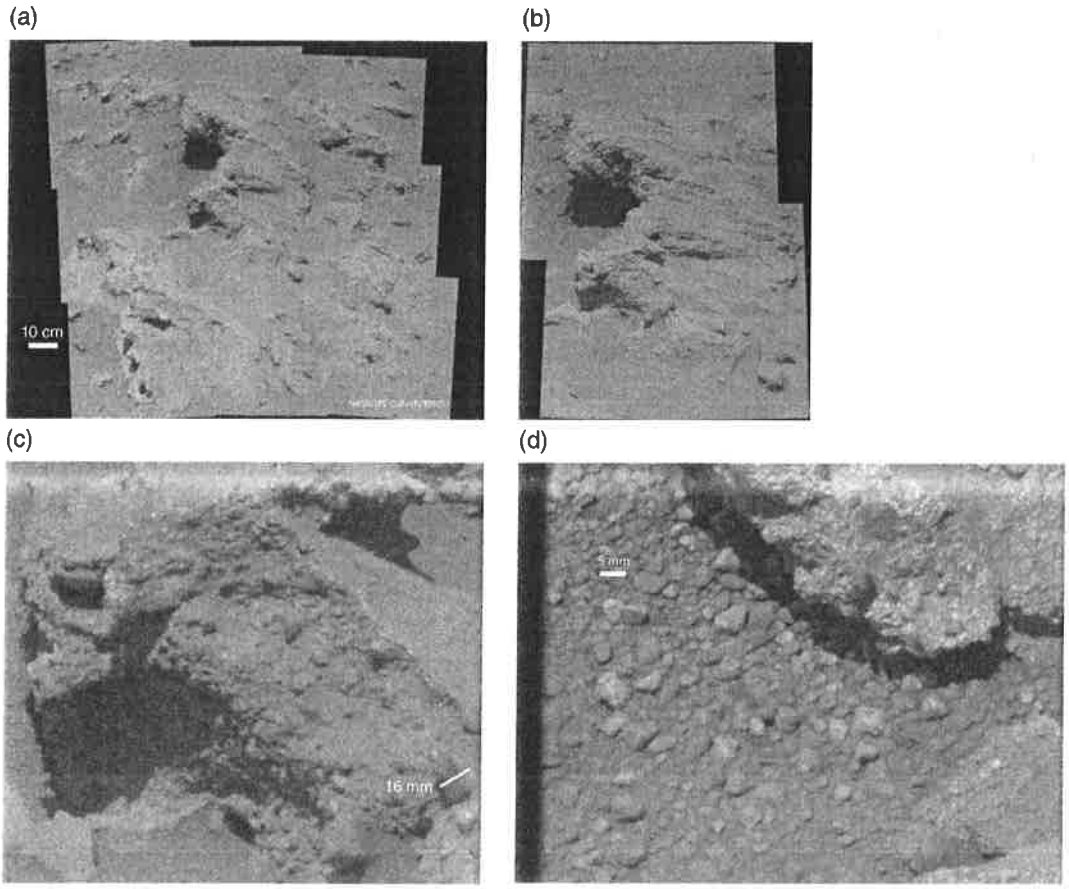


**Figure 28.2** (a) Fluvial conglomerates exposed near the *Curiosity* rover landing site. The outcrop is referred to as "Hottah" and this mosaic was taken by the Mastcam camera on Sol 039 (Mastcam images 0039MR0177000000E, 0039MR0177001000E1, 0039MR0177002000E1, 0039MR0177003000E1, 0039MR0177004000E1, 0039MR0177005000E1, 0039MR0177006000E1, 0039MR0177007000E1, and 0039MR0177008000E1). (b) Close-up view of the Hottah conglomerates. (c) A 16 mm pebble within the conglomerate is highlighted on the right side of the image. (d) A close up view of the conglomerate as well as pebbles inferred to have eroded out from the outcrop. Only abrasion during water transport can produce grains of this size, shape, and rounding and therefore appears to be definitive evidence of fluvial gravel transport.

## 28.3 Some Fluvial Conglomerates on the Way to Mount Sharp

The rover has driven over 10 km since landing, and conglomerates have been noted periodically throughout this drive to Mount Sharp. Every photograph taken by the Mars Science Laboratory is available at http://mars.jpl.nasa.gov/msl/multimedia/raw/. Figure 28.4 shows some examples of exposures and Figure 28.4d shows the travel path of the rover. Figure 28.4a is from the Yellowknife Bay area at the distal end of the Peace Vallis fan. The pebbles range from 2 to 8 mm in diameter. These stones are big enough to have low friction angles relative to the much finer sand, but not so big as to be immobile. In terrestrial studies isolated pebbles in the sand beds are known to occur well downstream of the gravel–sand transitions in rivers (e.g. Venditti and Church 2014). Figure 28.4b and c show coarse

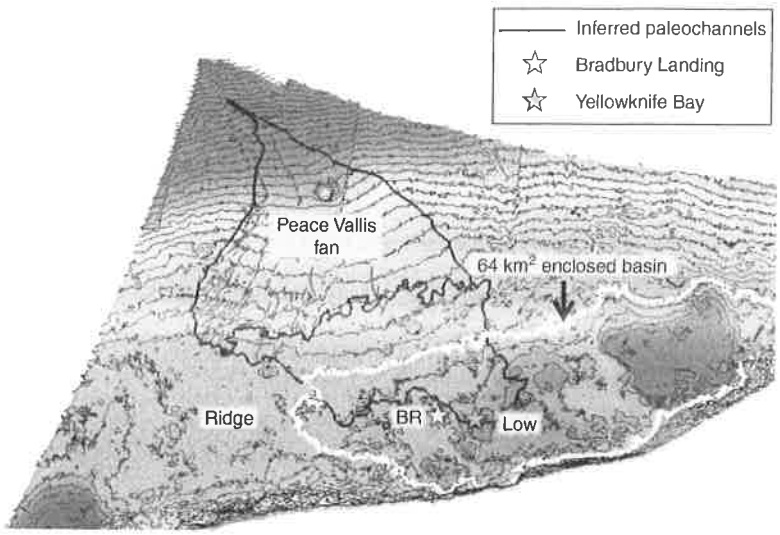


**Figure 28.3** A three-dimensional view of the Peace Vallis fan system (vertical exaggeration a factor of 10) with a colorized elevation map and 10 m HiRISE contours. Adjacent to the "Ridge" and within the enclosed basin (denoted by the thick white contour) is Bradbury Rise ("BR") and to the east of Bradbury Rise is a local low ("Low") into which the lower fan enters. The location of the MSL *Curiosity* rover landing site (Bradbury Landing) is indicated by the light star and Yellowknife Bay is indicated by the shaded star.

poorly sorted conglomerates about 6 km southwest from the landing site (near Kimberly in Figure 28.4d). The deposits are weakly lithified and the grains are rounded. The largest grains exceed 50 mm in size. In Figure 28.4b the outcrop was about 19 m from the rover and in Figure 28.4c the outcrop was about 13 m from the rover.

Work is currently underway to place these gravel deposits in a stratigraphic and geomorphic setting (Grotzinger *et al.* 2015). Below we first review how channel flows can be estimated if channel slope, grain size, and width are known. Gravel outcrops observed by *Curiosity*, however, reveal no discernable channel-scale features, i.e. width, depth, or slope. We then discuss how from just grain size alone crude estimates of channel scale and discharge can be made.

## 28.4 Estimates of Stream Velocity, Channel Discharge, and Gravel Mobility on Mars

Before the *Curiosity* rover landed and revealed the first direct observations of fluvial gravels on Mars, many studies had relied on satellite imagery to infer fluvial processes on Mars, specifically gravel transport. These studies exploited morphologic data (e.g. channel widths and slopes) and inferences about grain size to estimate bankfull channel flows, sediment transport rates, and durations of the fluvial period. Such analyses have been important in indicating periods of free-flowing water on Mars, and consequently, climatic conditions favorable for such conditions. Here we first discuss the varying strategies used to infer flow rates from morphologic evidence and then review the contrasting challenge presented by the *Curiosity* imagery to date: gravel outcrops, but no strong morphologic context to constrain flow conditions.

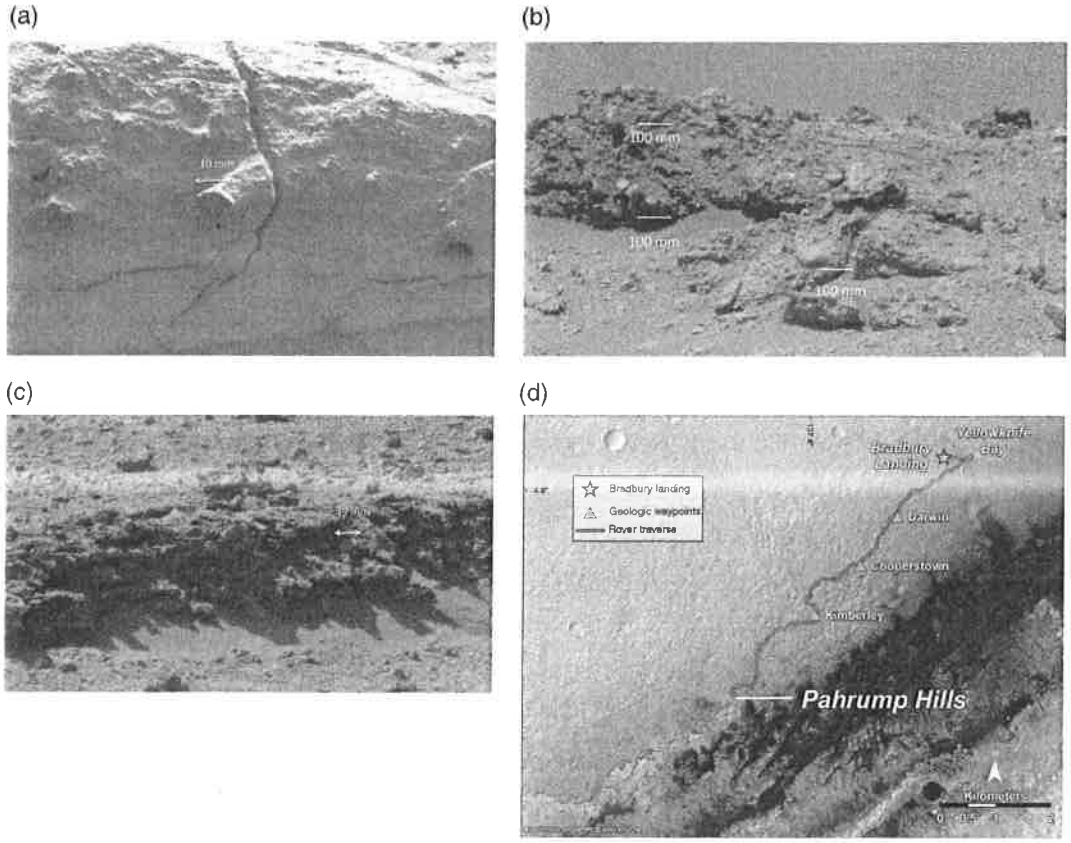


**Figure 28.4** Three examples of gravel exposures as observed by the Mastcam cameras on the *Curiosity* rover. (a) An image from Yellowknife Bay, taken on Sol 153 (Mastcam 100 MR0850001), showing isolated stones in poorly sorted sandstones. (b) Mastcam image (MR002747) taken on Sol 646 from Occum Pond location showing a coarse conglomerate. (c) Mastcam image (MR002462) taken on Sol 588 from Point Coulomb location showing another example of a coarse gravel conglomerate. (d) Drive path of the *Curiosity* rover. Image is available at NASA web page as Mars-MSL-curiosity-rover-location-map-pahrump-hills-pia18607-br2. (See insert for color representation of this figure.)

Standard hydraulic and sediment transport relations applied to terrestrial systems are often applied to Mars to estimate stream discharge and runoff rates (see reviews in Wilson *et al.* 2004; Kleinhans 2005; Irwin *et al.* 2008; Williams, Irwin, and Zimbelman 2009; Grotzinger *et al.* 2013). Two general approaches have been used to estimate channel-flow depth and velocity, and channel discharge on Mars: (i) the threshold channel concept and (ii) hydraulic geometry and river morphology correlations. The threshold channel concept assumes: (i) that gravel-bed material only starts to move significantly once a critical boundary shear stress is reached and (ii) this flow condition roughly corresponds to bankfull discharge. There is theory and observation to support this approach (e.g. Parker 1978; Andrews 1984; Dade and Friend 1998; Ryan, Porth, and Troendle 2005; Parker *et al.* 2007). In contrast, hydraulic geometry (i.e. empirical power law relationships between hydraulic properties of channels, such as bankfull width and depth, and stream discharge), first defined by Leopold and Maddock (1953), have been used as alternative means of estimating flows without making any assumptions about sediment transport conditions. Empirical power law morphologic scaling (e.g. meander

wavelength variation with channel width) has been used to infer morphologic properties that can then be used in hydraulic geometry relationships (e.g. Irwin *et al.* 2014). Although empirical studies under varying combinations of gravity, viscosity, and sediment and fluid density are not available, it is assumed that these simple scaling corrections can be applied to hydraulic geometry and morphologic correlations under Martian conditions (e.g. Irwin *et al.* 2008).

The system of equations most commonly used for estimating discharge in a channel with an observed channel width relies on the threshold channel concept, which is described in detail in section 28.4.1. By conservation of mass, discharge $Q$ equals the mean velocity $\bar{u}$ times depth $h$ times channel width $w$.

$$Q = \bar{u}wh \tag{28.1}$$

A widely used empiricism that relates mean velocity $\bar{u}$ to shear velocity $u_*$, where the shear velocity is defined as

$$u_* = \sqrt{\frac{\tau_b}{\rho}} = \sqrt{ghS} \tag{28.2}$$

($S$ is water surface slope, $\rho$ is fluid density and $g$ is gravity), is

$$\bar{u} = \left(\frac{8ghS}{f}\right)^{0.5} \tag{28.3}$$

In Equation (28.3), $f$ is a representative frictional resistance, which in this case is the Darcy–Weisbach friction factor.

There are numerous empirical expressions for the friction factor (e.g. Ferguson 2013). One that is intended to work for a range of flow conditions from shallow, boulder-rich channels to deeper flows over gravel is that proposed by Ferguson (2007). Morgan *et al.* (2014) write the Ferguson (2007) equation using the Ferguson reported empirical coefficients fit to data as

$$\left(\frac{8}{f}\right)^{0.5} = 17.7\frac{h}{D_{84}}\left[56.3 + 5.57\left(\frac{h}{D_{84}}\right)^{\frac{5}{3}}\right]^{-0.5} \tag{28.4}$$

in which $D_{84}$ is the grain size for which 84% of the particles sizes are smaller. This empirical fit was derived using data from a wide range of channel slopes (i.e. ~0.001 to ~0.2).

Flow depth, which appears in both Equations (28.1) and (28.4) to calculate velocity, is difficult to estimate on Mars. Many channels are canyons in which the flow during incision likely only occupied a portion of the total canyon depth. Width is more readily evident, although canyon widths can be misleading. Channels are commonly recognized by sinuous, relatively uniform width and flat-topped ridges (Figure 28.5; e.g. Williams, Irwin, and Zimbelman 2009; Burr *et al.* 2010). These inverted channels, in which cemented or armored beds are resistant to wind deflation compared to adjacent areas, may preserve channel width, but not directly reveal flow depth. Some theory or empiricism is typically needed to estimate depth and thus solve Equation (28.3).

### 28.4.1 Threshold Channel Concept

Terrestrial studies have found that in gravel-bedded channels significant bedload motion typically develops as flows approach bankfull discharge (e.g. Parker 2008). Furthermore, theory for gravel-bedded channels with gravel banks suggests that a stable channel cross-section, i.e. one that transmits

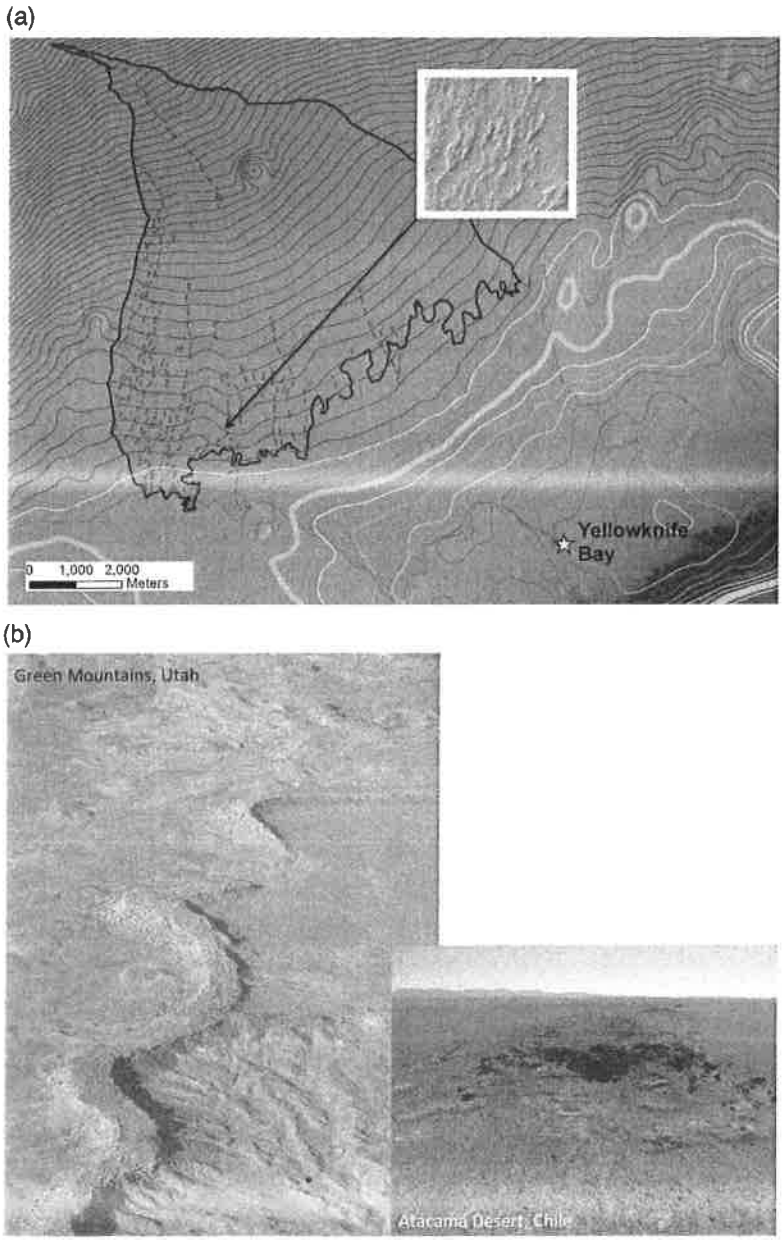


**Figure 28.5** (a) From HiRISE imagery, 43 distinct ridges were mapped on the Peace Vallis fan system (shown here on the lower fan region as dashed lines; 5 m contour interval); they varied in width from 5 to 130 m, with an average width of 27 m (Palucis *et al.* 2014). (b) Images of an inverted channel segment from the Green Mountains, Utah where channel widths are about 54 m (Williams, Irwin, and Zimbelman 2009) and the Atacama Desert.

bedload without significant bank erosion, occurs when the boundary shear stress is just slightly above a representative critical boundary shear stress for the initiation of motion (e.g. Parker 1978; Ikeda, Parker, and Kimura 1988; Parker *et al.* 2007; Seizilles *et al.* 2013). Consequently, it is commonly assumed that bankfull flow in gravel-bedded channels generates a boundary shear stress equal to the critical boundary shear stress. This threshold channel concept provides a means to specify a flow depth if channel slope and grain size can be estimated, and this then enables calculation of mean flow velocity, $\bar{u}$, and discharge. The critical Shields number for initial motion $\tau_{*cr}$ can be written as

$$\tau_{*cr} = \frac{\rho g h S}{(\rho_s - \rho) g D_{50}} \tag{28.5}$$

in which $\rho_s$ is the sediment particle density and $D_{50}$ is the median grain size of the bed surface. If we write the grain roughness scale in Equation (28.4) as $D_{84} = aD_{50}$, we can solve for the flow depth,

$$h = \tau_{*cr} \frac{(\rho_s - \rho)}{\rho a S} D_{84} \tag{28.6}$$

Lamb, Dietrich, and Venditti (2008) found that the critical Shield's number is slope dependent,

$$\tau_{*cr} = 0.15 S^{0.25} \tag{28.7}$$

and several papers support this finding (e.g. Prancevic, Lamb, and Fuller 2014). Substitution into Equation (28.6) leads to

$$h = 0.15 S^{-0.75} (P/a) D_{84} \tag{28.8}$$

in which $P$ is $\left(\frac{\rho_s - \rho}{\rho}\right)$.

Equation (28.8) implies that the flow depth at initial motion (which is the assumed bankfull flow depth) varies not quite inversely with slope and directly with the $D_{84}$. As Morgan *et al.* (2014) point out flow depth $h$ also will vary with the concentration of fine sediment in the fluid, which influences fluid density $\rho$: the higher the concentration, the shallower the depth.

By combining Equations (28.2), (28.4), (28.7), and (28.8), the mean velocity $\bar{u}$ is

$$\bar{u} = 1.028 S^{-0.625} (P/a)^{1.5} (D_{84} g)^{0.5} \left\{ 56.3 + 0.236 S^{-1.25} (P/a)^{1.667} \right\}^{-0.5} \tag{28.9}$$

Substitution of various values of slope, holding all other parameters constant, shows that mean velocity increases with decreasing slope, a result opposite from Equation (28.2) alone (without the critical shear stress constraint). This reduction is non-linear with much greater velocity increases as slope decreases from 0.03 to 0.01 than from 0.003 to 0.0003 (approaching the lower limit at which gravel-bedded rivers are found on Earth). With decreasing slope, for critical shear stress flow conditions to be met, the depth will increase. Also, converse to expectations without the critical boundary shear stress constraint, the mean velocity is predicted to increase with the bed roughness length scale $D_{84}$, specifically to the square root of that grain size. As many have pointed out (e.g. Irwin *et al.* 2008), the reduced gravity of Mars relative to Earth leads to lower velocities, i.e. velocity varies as the square root of gravity, as shown in Equation (28.9).

Substituting Equations (28.8) and (28.9) into Equation (28.1) leads to

$$Q = 0.154 w S^{-1.375} (P/a)^{2.5} {D_{84}}^{1.5} g^{0.5} \left\{ 56.3 + 0.236 S^{-1.25} (P/a)^{1.667} \right\}^{-0.5} \tag{28.10}$$

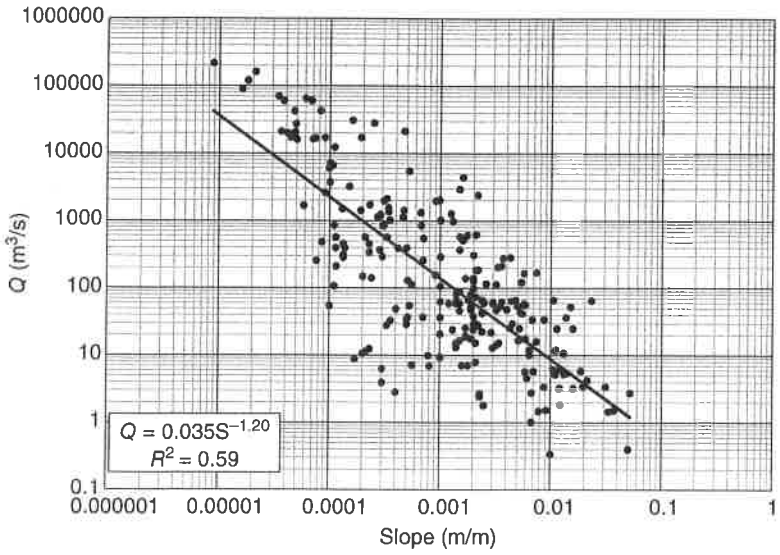


**Figure 28.6** Observed bankfull discharge versus channel slope for 230 sites compiled by Li *et al.* (2014). Discharge is inversely proportional to slope with a power law exponent of −1.2 and an $R^2$ value of 0.59.

which illustrates the relative importance of estimates of slope $S$, relative density $P$, and grain size in the calculation of channel discharge. Performing various substitutions in Equation (28.10) and plotting the results shows that $Q$ varies as an inverse power law of slope, with the power exponent ranging from −0.8 to −0.9. This is consistent with empirical correlations with terrestrial river systems. Figure 28.6 shows a plot of bankfull discharge versus channel slope from a recently published terrestrial river data compilation (i.e. Li *et al.* 2014). While the correlation is significant, the range of variation about the regression line for any particular slope value is two orders of magnitude. Substitutions into Equation (28.10) indicate that discharge depends on the relative density term $P$ to an exponent of about 2.5, but the range of probable values of $P$ is narrower than for $S$. Predicted discharge increases as the 1.5 power of $D_{84}$, thus an uncertainty of $D_{84}$ of an order of magnitude equates to a 32-fold uncertainty in discharge. Further constraints on likely flow depths can be to use empirical width to depth ratios for terrestrial rivers (e.g. Palucis *et al.* 2014).

An alternative equation often used in terrestrial studies to Equations (28.3) and (28.4) is the vertically integrated law of the wall equation, using an empirical grain-size roughness length scale of $3.5D_{84}$ (e.g. Garcia 2008)

$$\bar{u} = \frac{u_*}{k}\ln\left(\frac{11h}{3.5D_{84}}\right) \tag{28.11}$$

in which $k$ is von Karman's constant (0.4). Combining Equation (28.11) with (28.8) and setting the boundary shear stress equal to the critical boundary shear stress in calculating the shear velocity $u_*$, the velocity expression becomes,

$$\bar{u} = 0.968S^{0.125}(P/a)^{0.5}(D_{84}g)^{0.5}\ln\left(0.471S^{-0.75}(P/a)\right) \tag{28.12}$$

and the discharge is

$$Q = 0.145wS^{-0.625}(P/a)^{1.5}D_{84}{}^{1.5}g^{0.5}\ln\left(0.471S^{-0.75}(P/a)\right) \tag{28.13}$$

Equations (28.9) and (28.12) and (28.10) and (28.13) yield nearly identical results. Figure 28.7a shows the observed mean-velocity–flow-depth product for the rivers in the Li *et al.* (2014) compilation versus that predicted using Equation (28.13) divided by flow width. $P$ was specified as 1.65 and $a$ as 2.0 ($D_{84}$ was calculated from reported $D_{50}$ data). Only data for channels with a grain size of 10 mm or greater were used because the analysis by Li *et al.* (2014) showed that finer gravel-bedded rivers tend to have higher Shield's numbers $\tau_{*c}$. The threshold flow depths (and discharges) are consistently low

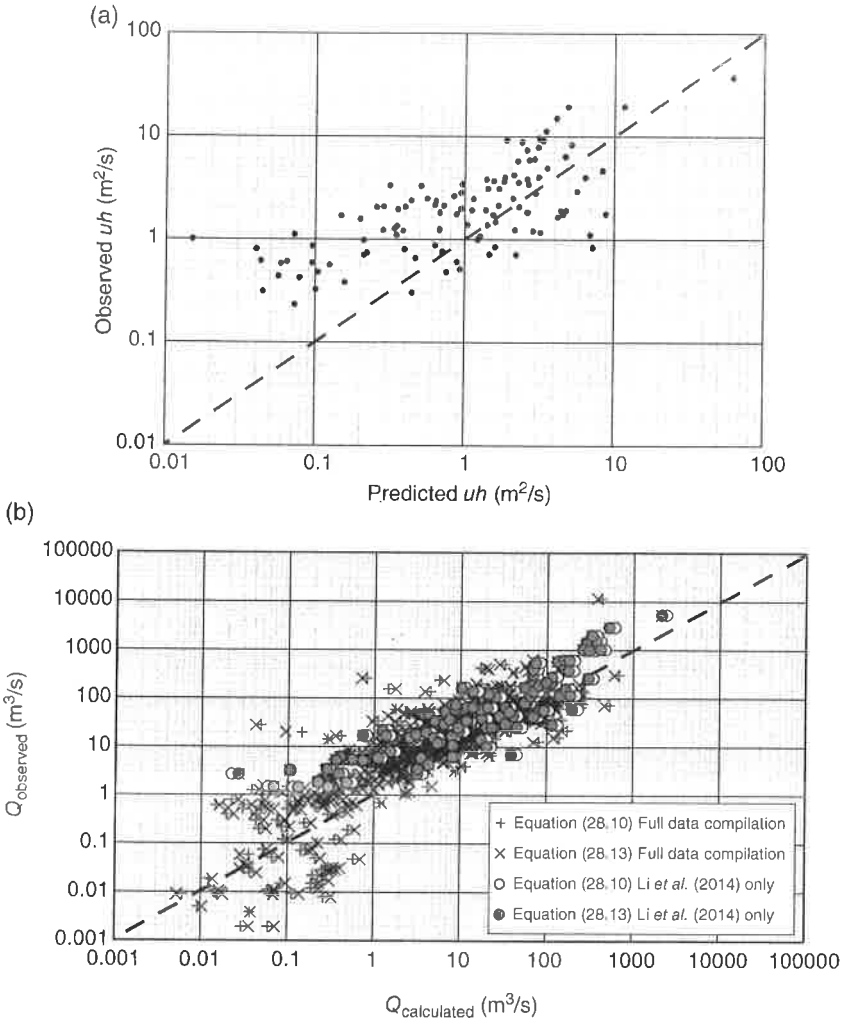


**Figure 28.7** (a) Observed velocity–depth product (*uh*) plotted against predicted velocity–depth product in units of ($m^2/s$) using the Li *et al.* (2014) data compilation for grains larger than 10 mm. Prediction is based on Equation (28.13) (for calculating $Q$) divided by channel width for the threshold channel case. Width is not included here to eliminate the improvement obtained by plotting width on both axes. While there is considerable scatter, the data systematically deviate to the left of the 1:1 line at lower velocity–depth products, i.e. Equation (28.13) divided by width underpredicts the velocity–depth product. (b) Comparison of observed versus predicted discharge from Equations (28.10) and (28.13) for 709 rivers (from a compilation of Li *et al.* (2014; 230 points shown in dots), Trampush, Huzurbazar, and McElroy (2014; 196 rivers distinct from Li *et al.*), and a new compilation with an additional 283 rivers).

for shallower channels, suggesting that the boundary shear stress at bankfull was above critical or that additional roughness scales matter. Figure 28.7b shows a plot of observed and predicted discharge (from Equations (28.10) and (28.13)) for two sets of data: the Li *et al.* (2014) data and a compilation of data from Li *et al.* (2014), Trampush, Huzurbazar, and McElroy (2014) and additional rivers compiled by the authors (a supplement spreadsheet of all data is provided). Results of Equations (28.10) and (28.13) show only small differences. For most of the discharge range, the calculated discharge is less than observed.

### 28.4.2 Hydraulic Geometry Applications

An alternative to the threshold channel approximation for estimating channel flows is to use empirical bankfull hydraulic geometry relationships (e.g. Irwin *et al.* 2008, 2014). Using data from 230 terrestrial river reaches, Li *et al.* (2014) found bankfull shear velocity, $u_{*bf}$, to be

$$u_{*bf} = 35S^{0.26}(Pg\nu)^{0.333} \tag{28.14}$$

where $\nu$ is the kinematic viscosity. The data did not have a wide range of viscosities reported, and all of the reaches had the same gravity, so the actual dependence on these two terms was not tested.

Since $u_{*bf} = (ghS)^{0.5}$, the depth dependence is

$$h_{bf} = 1220(P\nu)^{0.667}g^{-0.333}S^{-0.47} \tag{28.15}$$

This relationship has the advantage over Equation (28.8) in that it is not grain-size dependent and it corresponds empirically to terrestrial bankfull depth dependence on slope. It also introduces a viscosity dependence that raises questions about water temperature (and possible salt content) and sediment concentration at times of flow on Mars. Figure 28.8 shows observed versus predicted depth using Equation (28.15). Although Equation (28.14) is derived using the dataset from Li *et al.* (2014), there

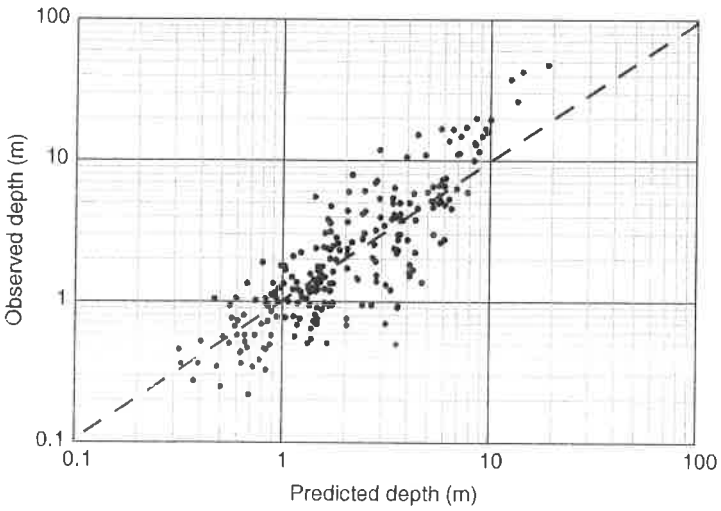


**Figure 28.8** Observed bankfull depth versus predicted bankfull depth using the shear velocity relationship (Equation (28.14)) reported by Li *et al.* (2014). The data begin to systematically deviate to the left of the 1:1 line as depth increases, i.e. the relation suggested by Li *et al.* (2014) underpredicts the actual depth. A minor correction to equation (28.14) was published by Li *et al.*, (2016), after this chapter was written. This correction is sufficiently small that it makes imperceptible changes to this Figure and Figure 28.9, hence the equations and corresponding plots were not replaced.

is a systematic residual underprediction at deeper channel depths, which is also visible in the figures reported in Li *et al.* (2014).

Equations (28.15) and (28.8) predict the same depth (and consequently the same velocity) when

$$D_{84} = 8133a\nu^{0.67}(Pg)^{-0.33}S^{0.28} \tag{28.16}$$

Equation (28.15) can also be used in roughness relationships to calculate velocity, as was shown above.

For the law of wall relationship (Equation (28.11)), the mean velocity is

$$\bar{u} = 87.3(Pg\nu)^{0.334}S^{0.265}\ln\left(3834(P\nu)^{0.667}g^{-0.33}S^{-0.47}D_{84}^{-1.0}\right). \tag{28.17}$$

Hence, if Equation (28.15) is used to estimate depth, a velocity calculation still requires a roughness estimate and consequently for gravel-bed channels a grain-size estimate. The discharge becomes

$$Q = 106506(P\nu)S^{-0.205}\ln\left(3834(P\nu)^{0.667}g^{-0.33}S^{-0.47}D_{84}^{-1.0}\right)w \tag{28.18}$$

There is a key distinction between the threshold channel approach and the use of empirical hydraulic geometry relationships. The bankfull hydraulic geometry, defined by Equations (28.17) and (28.18), predict opposite grain-size dependencies than the threshold channel model. All else held constant, mean velocity in (28.17) and discharge in (28.18) decreases with increasing grain size. Typically in terrestrial systems, however, the bed material coarsens with increasing slope (e.g. Ferguson *et al.* 1996; Montgomery and Buffington 1997; Dade and Friend 1998), such that flow velocity may vary little. For the recently reported Li *et al.* (2014) data, the median velocity value was about 1.52 m/s with a standard deviation of 0.73 m/s. This median value, corrected for reduced gravity (i.e. multiply by 0.61 (see Irwin *et al.* (2008)), may provide a useful first estimate of flow velocities.

Figure 28.9a shows observed and predicted velocity–depth products ($uh$) (Equation (28.18) divided by width). The scatter is large, reflecting both the systematic difference reported in Figure 28.8 and the poor predictability of velocity. A similar plot using a constant velocity of 1.52 m/s yields a better fit, but the range of observed values for any predicted $uh$ remains two orders of magnitude.

To use the above expressions on Mars to estimate depth, velocity, and discharge, particle density relative to fluid density $P$, water surface slope $S$, fluid viscosity $\nu$, and median or $D_{84}$ grain sizes must be estimated. Particle density in most cases is likely close to 3.0 g/cm$^3$ (i.e. density of basalt), but fluid density is not known (e.g. Morgan *et al.* 2014). Surface slopes, a proxy for water surface slope, can be estimated from well-defined features (e.g. fans, deltas, inverted channel paths) if they exist and topographic data are available, but must be estimated for deposits out of geomorphic context (see next section). Grain-size estimates have tended to favor fairly coarse gravels. Wilson *et al.* (2004) cite surface rock sizes observed by the Viking and Pathfinder missions when proposing a $D_{84}$ of 164 mm for calculations for outflow channel discharge analysis. Kleinhans, van de Kasteele, and Hauber (2010), in the absence of direct observations, have settled upon a $D_{50}$ of 100 mm, regardless of the context. Morgan *et al.* (2014) interpret HiRISE 0.25 m/pixel imagery of likely paleochannel bed surfaces as indicating a median grain size of 125–250 mm. While such grain sizes may be appropriate for slopes on the order of 1% in an alluvial setting, it seems highly probable to be in error in canyon settings where deep high flows can scour the channel to bedrock or boulders (as discussed by Irwin *et al.* (2014)), or on low-gradient alluvial features (less than 0.1%). Collectively, these uncertainties mean that discharge calculations using the systems of equations above are at least an order magnitude out, but two orders of magnitude is probably common. As shown in Figures 28.7b and 28.9b, even when applied to terrestrial rivers, the uncertainty about the actual discharge remains large.

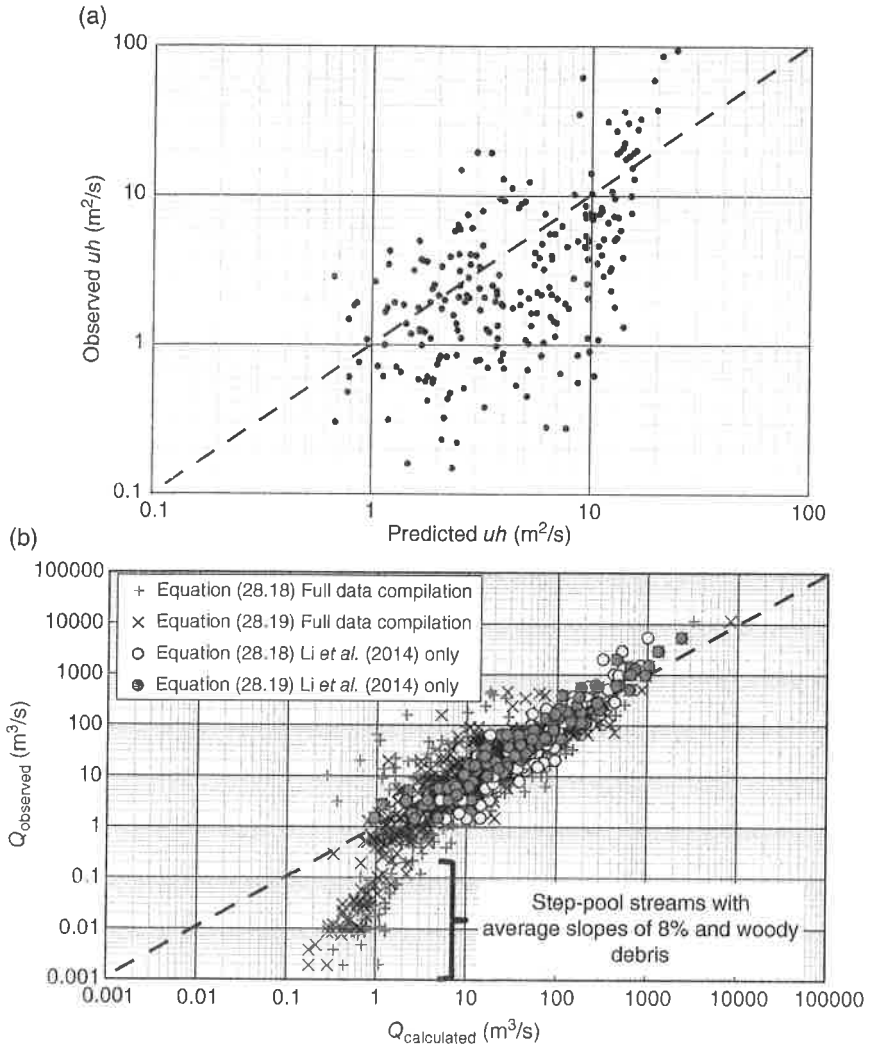


**Figure 28.9** (a) Observed velocity–depth product (*uh*) plotted against predicted velocity–depth product in units of ($m^2/s$) using the Li *et al.* (2014) data compilation for all grain sizes. Prediction is based on Equation (28.18) (the hydraulic geometry case) divided by channel width. The scatter about the 1:1 line is large, due to both the differences reported in Figure 28.7 and the difficulty in predicting velocity. (b) Comparison of observed versus predicted discharge from Equations (28.18) and (28.19) for 709 rivers (from a compilation of Li *et al.* (2014; 230 points shown in colored dots), Trampush, Huzurbazar, and McElroy (2014; 196 rivers distinct from Li *et al.*), and a new compilation with an additional 283 rivers). The data points that obviously deviate from the 1:1 line are steep, step-pool streams located in the American west (namely Washington State and Montana) that have large amounts of woody debris (data from Wohl and Merritt 2005).

The most direct application of hydraulic geometry in Martian settings, one that avoids estimating parameters, is to use terrestrial correlates between bankfull discharge (corrected for Martian gravity) and bankfull width. For example, Irwin *et al.* (2014) measured meander geometry of the large channel bends in Eberswalde delta to estimate channel width and then used a correlation between the 2 year

recurrence interval discharge event (corrected for Martian gravity) and bankfull width from the Missouri River Basin, a region inferred to have low bank strength, to estimate the discharge in the Eberswalde meanders. Two compilations of terrestrial data (with significant overlap in sources) provide data that yield these correlates (no gravity correction applied):

$$Q = 0.219w^{1.65} \tag{28.19}$$

from Li *et al.* (2014) representing 230 data points, and

$$Q = 0.134w^{1.72} \tag{28.20}$$

from Trampush, Huzurbazar, and McElroy (2014) representing 323 data points. The range of discharge values for a given width in these correlations is about an order of magnitude. Figure 28.9b shows the observed discharge plotted against the calculated discharge using Equations (28.18) and (28.19). The Li *et al.* (2014) data, which were used to parameterize Equations (28.18) and (28.19), are shown as circles, and the match is fairly close. The Trampush, Huzurbazar, and McElroy (2014) data plot similarly, but a subset of the data, collected on steep, step-pool channels, plot distinctly off the trend of the other data. These streams, which were originally studied by Wohl and Merritt (2005) and located in the western United States (Washington and Montana), were found to include abundant wood that could be altering channel morphologies. Figure 28.10 shows the observed discharge as a function of the channel width for combined data set in Li *et al.* (2014), Trampush, Huzurbazar, and McElroy (2014), and the compilation for this paper (a total of 654 unique data points, excluding the Wohl and Merritt (2005) data). The regression has an $R^2$ of 0.9,

$$Q = 0.20w^{1.66} \tag{28.21}$$

Geomorphic setting (canyon versus floodplain bordered), relative sediment supply and size, bank strength controls, vegetation, and runoff characteristics can cause specific locations to differ greatly from these broad empirical trends, hence application to studies on Mars, while perhaps useful, must be considered approximate. It is not obvious that using Equation (28.19), (28.20), or (28.21) based on

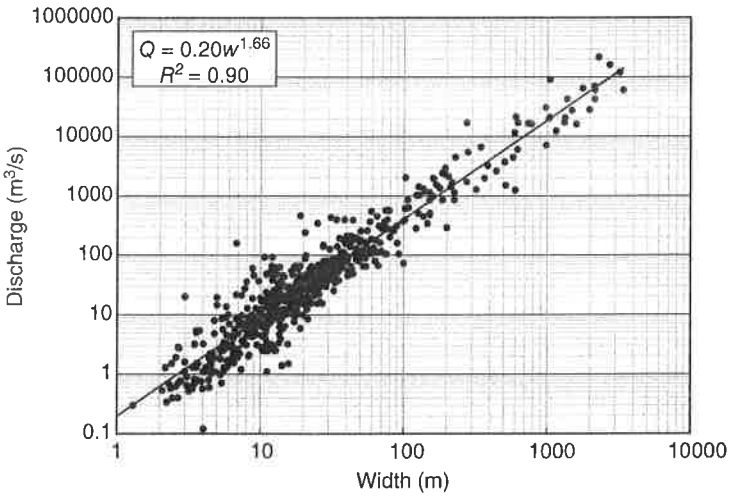


**Figure 28.10** Bankfull discharge as a function of bankfull width for 654 river sites (excluding the data from Wohl and Merritt 2005).

width observations alone, yields a poorer estimate of discharge than the more mechanistic relationships described above.

### 28.4.3 Analysis of Martian Gravel Conglomerates

The gravel conglomerates directly observed on Mars with the *Curiosity* rover offer the opposite problem to that outlined in sections 28.4.1 and 28.4.2. In Gale Crater we can estimate grain sizes in the relatively thin exposures revealed in transit towards Mount Sharp, but we do not see channel widths and preserved channel slopes. There is no direct surface morphologic guide to estimating flows. This is the common circumstance for gravel deposits in the rock record on Earth as well, and strategies for estimating channel slope have been proposed for gravel (e.g. Paola and Mohrig 1995) and sand deposits (e.g. Lynds *et al.* 2014), although in both cited cases the flow depth must be determined from stratigraphic relationships.

Williams *et al.* (2013), in reporting on the first fluvial conglomerates on Mars, did grid by number counts on the thin exposed edges of cemented gravels to obtain grain-size distributions. The median grain size for three separate outcrops range from 4.5 to 9.5 mm and the corresponding $D_{84}$ is 6.5 to 15 mm. They estimated the minimum flow to transport the gravels for the threshold channel for initial motion case, and used Equation (28.5) with two bracketing values of the critical Shields number (0.03 and 0047) and two estimated water surface slopes (0.01 and 0.001) to estimate flow depth (Equation (28.6) using the observed $D_{50}$ and velocity (from Equation (28.11)). The slope estimates were based on the slope of the nearby Peace Vallis fan, the lower portion of which has a mean slope of about 0.01, and the empirical observation that gravel-bedded streams are typically steeper than 0.001. This led to bracketing depths and velocities between 0.27–0.89 m and 0.2–0.75 m/s, respectively.

Similar to the threshold versus hydraulic geometry approach to estimating flow properties described in the previous sections, empirical correlations provide another means of estimating flow properties when only grain size is known. The empirical compilations by Li *et al.* (2014) and Trampush, Huzurbazar, and McElroy (2014) show an approximate correlation between slope and median grain size in their selected terrestrial rivers (Figure 28.11a and b). For gravel sizes, especially 5–10 mm and coarser, there is essentially no relationship between slope and grain size. As many others have noted, rivers with grain sizes between 2 and 5 mm are rare (e.g., Venditti and Church 2014). According to Figure 28.11, for the grain sizes first observed at Gale Crater (i.e. 4.5–9.6 mm), a slope estimate of 0.001 to 0.01 appears to well represent the majority of the sites included in these terrestrial data sets. Notable exceptions to these slopes are the steeper, fine-grained fans studied by Stock *et al.* (2007) (and not included in either data compilation). Trampush, Huzurbazar, and McElroy (2014) report a correlation in which slope depends strongly on bankfull depth and weakly on grain size, but recommend the use of this correlation only for slopes less than $5 \times 10^{-3}$. They also note explicitly that their correlation should not be used for paleoslope analysis on Mars because it is strictly empirical and it is not established how fluid viscosity, density, and gravity may influence these relationships. In the absence of stratigraphic evidence of flow depth, however, only grain size can provide a guide to the scale of the flows that created the deposits imaged by *Curiosity*, and we can either guess based on terrestrial experience, use theory (which retains some level of empiricism in it), or use empirical relations with awareness for a need for caution.

If grain size can be used to estimate crudely the slope, then correlations with slope can point to channel dimensions. In the Li *et al.* (2014) data, bankfull channel depth varies inversely with slope (Figure 28.12),

$$h = 0.0567 S^{-0.52} \tag{28.22}$$

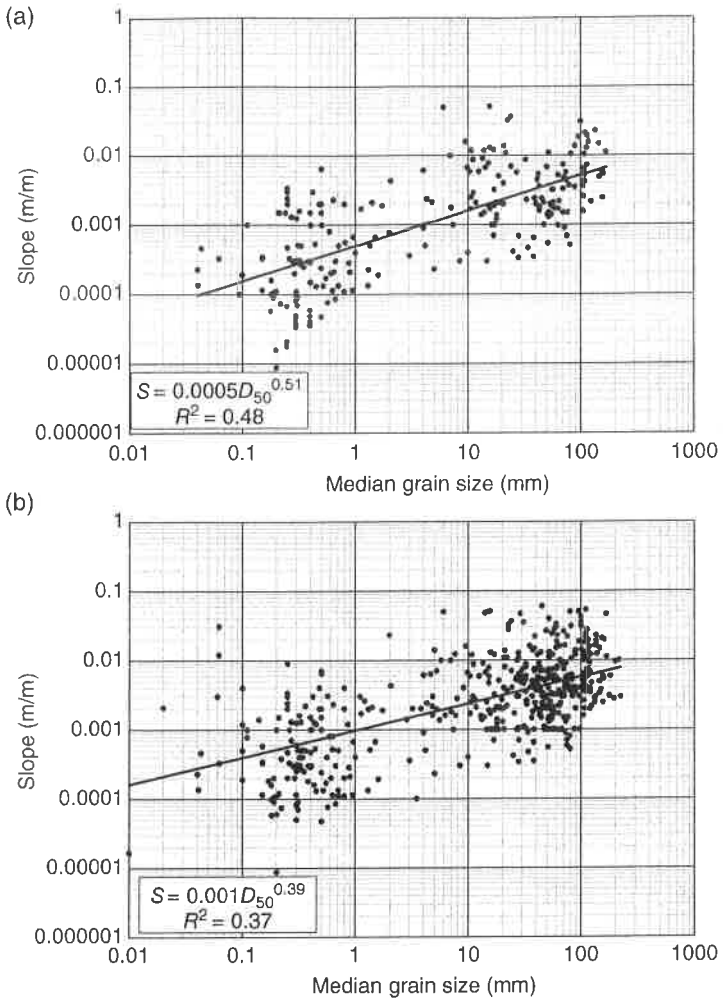


**Figure 28.11** (a) Channel slope as a function of grain size using data compilation by Li *et al.* (2014). While there is considerable variability in the median grain size for a given slope, the data follow a general trend where slope is proportional to $D_{50}$ raised to the one-half power. Reproduced with permission of Taylor & Francis.) (b) Channel slope as a function of grain size using data compilations by Trampush, Huzurbazar, and McElroy (2014). Again, while there is considerable variability in the median grain size for a given slope, the data follow a general trend where slope is proportional to $D_{50}$, though with this larger data set, the power law exponent is lowered to 0.4.

The $R^2$ is 0.73, but for slopes less than $6 \times 10^{-5}$ the depths are systematically underpredicted. This slope corresponds to depths greater than about 10 m. A channel slope of 0.01 would predict a bankfull depth of 0.62 m, and a slope of 0.001 would predict a depth of 2.1 m. These depths are higher than those estimated from the limiting case of threshold of motion (i.e. Williams *et al.* (2013) report a depth range of 0.03–0.09 m for a slope of 0.01 and 0.27–0.89 m for a slope of 0.001). Because the deposits could record transport conditions well above threshold, and because of additional roughness in the channel other than skin friction scaled by $D_{84}$, these deeper flows – though strictly empirically

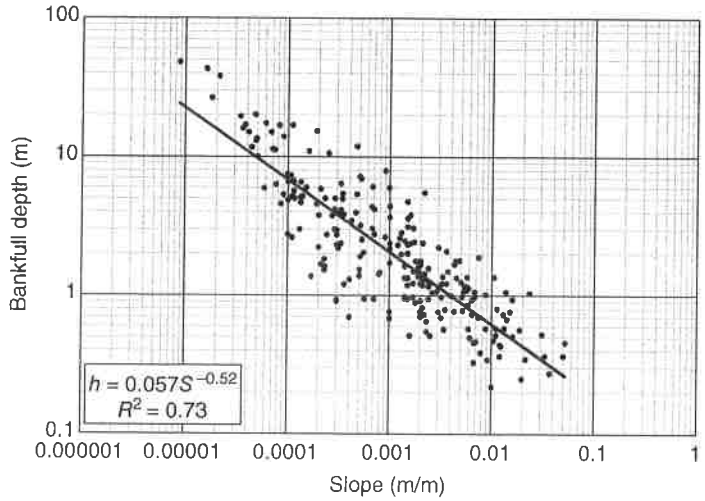


**Figure 28.12** Bankfull depth as a function of slope using the Li *et al.* (2014) data compilation. Bankfull depth is inversely proportional to slope, with a power law exponent of −0.52.

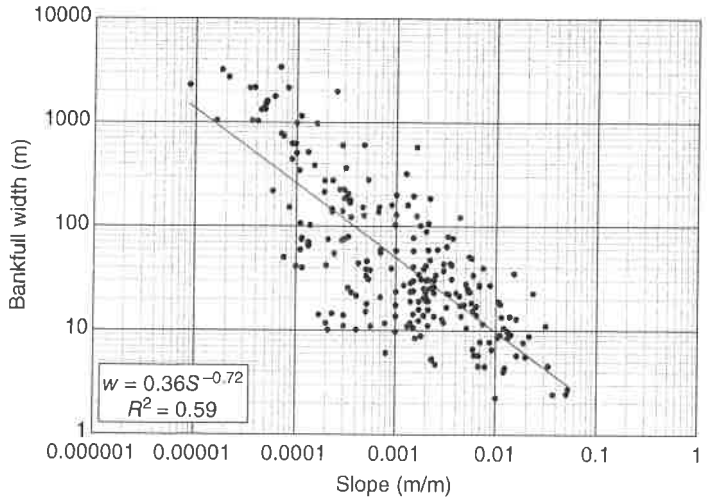


**Figure 28.13** Bankfull width as a function of slope for the Li *et al.* (2014) data.

derived – may be better estimates. Similarly, the Li *et al.* (2014) data lead to a bankfull width to slope correlation of

$$w = 0.36S^{-0.72} \tag{28.23}$$

The $R^2$ is lower (0.59) and there is systematic underprediction of width below slopes of $10^{-4}$ (Figure 28.13). For any given slope, the range of observed slope is about an order of magnitude, so this correlation provides only crude guidance to flow scale. It suggests that slopes of 0.01 would

typically have widths of about 10 m, and if the slope were reduced to 0.001, the width would be about 50 m.

Taking these empiricisms together, the fluvial conglomerates first documented by Williams *et al.* (2013) may have been deposited by a channel of about 0.62–2.1 m deep, 10–50 m wide, and if we assume the median flow velocity of terrestrial rivers reported in the Li *et al.* (2014) data set and correct for gravity (giving a mean velocity of 0.9 m/s) then the predicted discharge is about 5.6–94.5 $m^3/s$. Given the slope and depths, velocity could alternatively be calculated from Equation (28.9). If the estimated widths are used in the empirical discharge correlation with width for the Li *et al.* (2014) data set, the predicted bankfull discharges are 6 and 85.6 $m^3/s$ for the 10 and 50 m channel widths, respectively. This falls in the range of 3.7–207 $m^3/s$ estimated by Palucis *et al.* (2014) for channels on the nearby Peace Vallis fan. This analysis alone, cannot rule out, however, the possibility that the flows only slightly exceed threshold conditions and were relatively shallow and associated with poorly confined flows or sheet floods. Exposures that provide stratigraphic clues about flow depth will be particularly important in providing greater constraint on the character of the flows that transported the gravels observed in Gale.

## 28.5 Runoff Volume and Implications for Climate

The discharge analysis above provides only a sense of scale of the channel and the instantaneous bankfull flow. While peak flows from a given watershed area places constraints on possible runoff generation mechanisms, such as snow melt, rainfall-runoff, or impact melting of subsurface ice (e.g. Mangold *et al.* 2012; Morgan *et al.* 2014; Palucis *et al.* 2014), it does not reveal how much total runoff occurred to create a given fluvial feature.

Four recent examples illustrate the approaches taken to estimate total runoff volume on Mars. Mangold *et al.* (2012) employ a numerical model for delta construction by Kleinhans *et al.* (2010) to calculate a steady-state discharge of $8.7 \times 10^4$ $m^3/s$ feeding the construction of Eberswalde delta, a site of many investigations directed at runoff and sediment transport (e.g. Malin and Edgett 2003; Moore *et al.* 2003; Jerolmack *et al.* 2004; Bhattacharya *et al.* 2005; Wood 2006; Lewis and Aharonson 2006; Pondrelli *et al.* 2008; Rice *et al.* 2011; Mangold *et al.* 2012; Irwin *et al.* 2014). Mangold *et al.* (2012) assume a constant feeder channel in a canyon 500 m wide, 25 m deep with a gradient of 0.034 and a surface grain size of only 100 mm. Assuming various sediment to water ratios (0.05–30%), Mangold *et al.* (2012) suggested that the 5 $km^3$ delta could be built in 2 weeks to two decades. The total water volume to build the delta for a 5000 $km^2$ source area would be as high as 2 km to as low as 3 m (for the exceptionally dense flows with high sediment to water ratios). The calculated steady-state discharge to the delta is about 40% of the mean daily discharge on the Amazon River even though the watershed area that drains to the Eberswalde delta is just 0.3% of that of the Amazon. The annual sediment load would also exceed that currently discharged from the Amazon River (about $1200 \times 10^6$ t/yr, Syvitski *et al.* (2003)). Irwin *et al.* (2014) offer a detailed analysis that disagrees with the Mangold *et al.* (2012) proposals, and instead argue for a relatively long-lived hydrologic period to build the meandering channels, avulsing delta system, and sustained lake level.

Irwin *et al.* (2014) calculate the runoff rate to Eberswalde delta needed to maintain a constant lake level despite evaporation losses. Their estimate ranged from 2.4–16 cm/yr of runoff production. To deposit the estimated 6 $km^3$ of delta sediment, they estimate it would take 1–10 km of runoff for a 5000 $km^2$ contributing area to 0.4–4 km for a 17 000 $km^2$ contribution area. This may have occurred over $10^4$–$10^5$ years.

Morgan *et al.* (2014) estimate the volume of two intersecting fans in Saheki Crater to be 586 $km^3$. Assuming a sediment to water ratio in the runoff producing the fan of 0.2, they estimate that about 3.57 km of runoff was needed from the 793 $km^2$ watershed source area. This high sediment to water ratio is supported by the visibly coarse texture of the wind-exposed fan.

Palucis *et al.* (2014) estimate the volume of the Peace Vallis fan to be 0.93 $km^3$. They note that the sediment to water ratio in Chilean streams representing arid zones was reported to be about 0.0002 (Pepin *et al.* 2010). This leads to an estimate of 4650 $km^3$ of water runoff from the 730 $km^2$ watershed source area, or the equivalent of 6.4 km of runoff. Here we use a compilation of sediment yield and runoff data from 411 rivers (http://csdms.colorado.edu/wiki/Data:World_River_Sediment_Yields_-Database) to calculate the sediment to water ratio (assuming the bulk density of the deposited sediment is 1.9 $t/m^3$). The median value of the log-transformed data is −3.48, or a sediment to water ratio of 0.00033. Figure 28.14 shows the frequency distribution of log-transformed sediment to water volume ratios. When this sediment to water ratio is applied to the Peace Vallis fan system, it would suggest 3.9 km of runoff. Conservatively, Palucis *et al.* (2014) proposed that at least 0.6 km of runoff must have occurred to produce the fan.

In each of these cases, kilometers of total runoff from the watershed source areas are required to produce the observed depositional features. Note that evaporation and infiltration losses during runoff are not considered, so these numbers are likely minimum values. Because there cannot be kilometers of water equivalent stored as snow in these watersheds, this implies that the depositional features require a hydrologic cycle in which precipitation replenishes runoff. Morgan *et al.* (2014), for example, suggest that could be accomplished by an annual snow accumulation of about 3 m. Collectively, these analyses point to the need to have periods of 1000–100 000 year time scales of climatic conditions that support an active liquid hydrologic cycle on Mars. At each of the three sites, the timing of the fan/delta deposition may be similar (late Hesperian to early Amazon, i.e. 3.4–2.7 billion years ago), and thus may record the same climatic incident. Currently climate models have not been able to produce wet periods of this duration and magnitude.

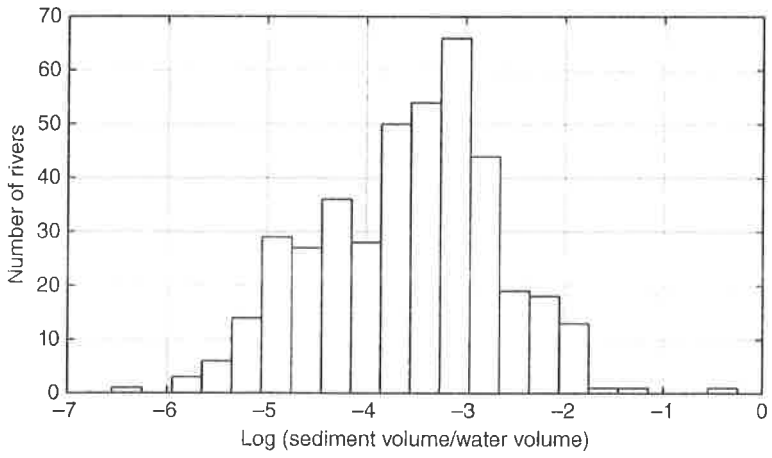


**Figure 28.14** Distribution of log-transformed sediment volume to water volume ratio for 411 rivers of the world. Sediment yield was converted to sediment volume assuming a density of 2650 $kg/m^3$ and a solid fraction of 0.7 (i.e. porosity of 0.3 for gravel).

## 28.6 Conclusions

The paleocanyon channels, meandering rivers, fans, and deltas on Mars have typically been assumed to be gravel bedded. Satellite imagery enabled quantification of fluvial forms, giving estimates of channel widths and slopes. The threshold channel concept and hydraulic geometry relationships based on analysis of terrestrial rivers have been used to estimate channel-flow characteristics including depth, velocity, and bankfull discharge. The threshold channel approach is conservative in that it assumes that flows only just reach critical shear stress at bankfull, and terrestrial studies show that finer gravel beds may tend to have higher shear stresses. This approach has the advantage that it has a theoretical foundation and a minimum of parameters, but it requires an estimate of bed-surface grain size and currently satellite imagery cannot resolve particles smaller than boulders. Consequently, grain sizes are typically guessed. The hydraulic geometry employs empirical power law relationships derived from metadata analysis of terrestrial rivers. Channels are not assumed to be just at threshold of motion, but if mean flow velocity is to be estimated, bed-surface grain size still must be guessed. The simplest approach is to use coarse correlates, such as the power law relationship between bankfull discharge and bankfull width. While the correction for gravity differences can be computed in hydraulic geometry relationships, the influence of fluid density, viscosity, and possible changes in erosional mechanics due to velocity–depth–shear-stress differences have an unknown effect on the relevance of terrestrial river hydraulic geometry relationships to Mars. Uncertainty in discharge estimates, even when applying empirical relationships to terrestrial data, remains large. In application to Mars, uncertainty of plus or minus an order of magnitude may be common.

The images returned from the *Curiosity* rover provide the first direct observations of fluvial conglomerates. The deposits are finer (order 10 mm) than has been assumed in satellite-based studies (100 mm). The stones vary in rounding, but some are quite well rounded, providing strong evidence of their fluvial history. Given the fine pebble size of the gravels exposed, the fluvial system responsible for transport was likely in a relatively low-gradient system (below 1%) with small channels (<50 m wide). Although we can quantify grain size, we then have to estimate paleoslope and flow depth. Terrestrial slope dependency on grain size, and width and depth dependence on slope in rivers provide one way to estimate paleochannel characteristics in the conglomerates. Analysis of photographs taken by *Curiosity* is underway to seek further observations to constrain the paleoenvironment of these fluvial deposits. Unlike sandstones, which can be of fluvial or eolian origin, gravel conglomerates provide definitive evidence of free-flowing surface water on Mars.

Total runoff to produce a specific deposit is very important to estimate, as it provides significant constraints on the climate conditions required. We have not documented the volume of water responsible for depositional landforms on Earth. On Mars, this estimate relies on assumptions about the sediment concentration in runoff. For the Earth, the median concentration of all the major rivers of the world is $\sim 10^{-4}$. Very high concentrations (upwards of 30%) have been proposed, but would seem incompatible in systems with well-defined sinuous low-gradient channels. In studies of fan/delta features recently published, the runoff from source areas has been estimated to be on the order of 1 km, thus requiring a period with a sustained hydrologic cycle (annual precipitation in source areas and runoff to areas of deposition) lasting likely thousands of years. A large uncertainty is the intermittency of the climate conditions favorable for runoff. Channel morphology places constraints, however, on the scale of runoff, and coupled with the total runoff required to produce a deposit, forces fluvial deposition events to extend to periods of at least thousands of years. These sites may have been fluvially active in the same period, about 3 billion years ago, sufficiently late in Mars' history that climate models do not expect an active liquid-water-driven hydrologic cycle.

## Acknowledgments

This research was conducted for the Jet Propulsion Laboratory, California Institute of Technology, under a contract to Malin Space Sciences Systems with NASA under the Mars Program Office. Martin Kleinhans and Aileen Yingst provided valuable reviews. Photographic images collected by the Mars Science Laboratory MAHLI/Mastcam/MARDI group led by the Malin Space Sciences Systems are revealing the fluvial history of Mars. We also thank the teams responsible for the orbital data, namely, the HiRISE, CTX, and HRSC teams.

## References

Andrews, ED 1984. Bed-material entrainment and hydraulic geometry of gravel-bed rivers in Colorado. *Geol. Soc. Am. Bull.* 95, 371–378.

Bhattacharya, JP, Payenberg, THD, Lang, SC, and Bourke, M 2005. Dynamic river channels suggest a long-lived Noachian crater lake on Mars. *Geophys. Res. Lett.* 32, L10201. http://dx.doi.org/10.1029/2005GL022747.

Burr, DM, Williams, RME, Wendell, KD *et al.* 2010. Inverted fluvial features in the Aeolis/Zephyria Plana region, Mars: Formation mechanism and initial paleodischarge estimates. *J. Geophys. Res.* 115, E07011. DOI:10.1029/2009JE003496.

Carr, MH 2012. The fluvial history of Mars. *Philos. Trans. R. Soc. A.* 370, 2193–2215. DOI:10.1098/rsta.2011.0500.

Carr, MH and Clow, GD 1981. Martian channels and valleys: Their characteristics, distribution, and age. *Icarus* 48(1), 91–117.

Carter, J, Loizeau, D, Mangold, N *et al.* 2015. Widespread surface weathering on early Mars: a case for a warmer and wetter climate. *Icarus* 248, 373–382.

Craddock, RA and Howard, AD 2002. The case for rainfall on a warm, wet early Mars. *J. Geophys. Res.* 107. DOI:10.1029/2001JE001505.

Dade, W and Friend, PF 1998. Grain-size, sediment-transport regime, and channel slope in alluvial rivers. *J. Geol.* 106(6), 661–676.

Fasset, CI and Head, JW 2008. Valley network-fed, open-basin lakes on Mars: distribution and implications for Noachian surface and subsurface hydrology. *Icarus* 198, 37–56. DOI:10.1016/j.icarus.2008.06.016.

Ferguson, R 2007. Flow resistance equations for gravel- and boulder-bed streams. *Water Resour. Res.* 43, W05427. http://dx.doi.org/10.1029/2006WR005422

Ferguson, R 2013. Reach-scale flow resistance. In *Treatise on Geomorphology*, Vol. 9 (ed. Wohl, E). Academic Press: San Diego, CA; 50–68.

Ferguson, R, Hoey, T, Wathen, S, and Werritty, A 1996. Field evidence for rapid downstream fining of river gravels through selective transport. *Geology* 24(2), 179–182.

García, MH 2008. Sediment transport and morphodynamics. *Sedimentation Engineering: Processes, Measurements, Modeling, and Practice*, Vol. 110 (ed. García, MH). American Society of Civil Engineers: Reston, VA; 21–164.

Grotzinger, JP, Hayes, AG, Lamb, MP, and McLennan, SM 2013. Sedimentary processes on Earth, Mars, Titan, and Venus. *Comparative Climatology of Terrestrial Planets* (eds Mackwell, SJ *et al.*). University of Arizona: Tucson.

Grotzinger, JP, Gupta, S, Rubin, DM *et al.* 2015. Deposition, exhumation, and paleoclimate of an ancient lake deposit, Gale Crater, Mars. *Science* 350(6257), 1–12. DOI:10.1126/science.aac7575.

Gulick, VC 1998. Magmatic intrusions and a hydrothermal origin for fluvial valleys on Mars. *J. Geophys. Res. Planets* 103(E8), 19365–19387. DOI:10.1029/98JE01321.

Gulick, VC and Baker, VC 1990. Origin and evolution of valleys on Martian volcanoes. *J. Geophys. Res. Solid Earth* 95(B9), 14325–14344. DOI:10.1029/JB095iB09p14325.

Ikeda, S, Parker, G, and Kimura, Y 1988. Stable width and depth of straight gravel rivers with heterogeneous bed materials. *Water Resour. Res.* 24, 713–722.

Irwin III, RP, Craddock, RA, and Howard, AD 2005a. Interior channels in Martian valley networks: discharge and runoff production. *Geology* 33(6), 489–492. http://dx.doi.org/10.1130/G21333.1

Irwin III, RP, Howard, AD, Craddock, RA, and Moore, JM 2005b. An intense terminal epoch of widespread fluvial activity on early Mars: 2. Increased runoff and paleolake development. *J. Geophys. Res.* 110, E12S15. http://dx.doi.org/10.1029/2005JE002460

Irwin, RP, Lewis, KW, Howard, AD, and Grant, JA 2014. Paleohydrology of Eberswalde crater, Mars. *Geomorphology*, http://dx.doi.org/10.1016/ j.geomorph.2014.10.012.

Jerolmack, DJ, Mohrig, D, Zuber, MT, and Byrne, S 2004. A minimum time for the formation of Holden Northeast fan, Mars. *Geophys. Res. Lett.* 31, L21701. http://dx.doi.org/10.1029/2004GL021326

Kleinhans, MG 2005. Flow discharge and sediment transport models for estimating a minimum timescale of hydrological activity and channel and delta formation on Mars. *J. Geophys. Res, Planets* 110(E2), E12003.

Kleinhans, MG, van de Kasteele, HE, and Hauber, E 2010. Palaeoflow reconstruction from fan delta morphology on Mars. *Earth Planet. Sci. Lett.* 294, 378–392. http://dx.doi.org/10.1016/j.epsl.2009.11.025

Lamb, MP, Dietrich, WE, and Venditti, JG 2008. Is the critical Shields stress for incipient sediment motion dependent on channel-bed slope? *J. Geophys. Res. Earth Surface* 113, F02008. DOI:10.1029/2007JF000831.

Le Deit, L, Hauber, E, Fueten, F *et al.* 2013. Sequence of infilling events in Gale Crater, Mars: Results from morphology, stratigraphy, and mineralogy. *J. Geophys. Res. Planets*. DOI:10.1002/2012JE004322

Leopold, LB and Maddock,T 1953. *The Hydraulic Geometry Of Stream Channels And Some Physiographic Implications*. Professional Paper 252, US Geological Survey; Washington, DC.

Lewis, KW and Aharonson, O 2006. Stratigraphic analysis of the distributary fan in Eberswalde crater using stereo imagery. *J. Geophys. Res.* 111, E06001. http://dx.doi.org/10.1029/2005JE002558

Li, C, Czapiga, MJ, Eke, EC *et al.* 2014. Variable Shields number model for river bankfull geometry: bankfull shear velocity is viscosity-dependent but grain size-independent. *Journal of Hydraulic Research*. DOI:10.1080/00221686.2014.939113.

Li, C, Czapiga, MJ, Eke, EC *et al.* 2016. Closure to "Variable Shields number model for river bankfull geometry: bankfull shear velocity is viscosity-dependent but grain size-independent" *Journal of Hydraulic Research*. DOI:10.1080/00221686.2015.1137088

Lynds, RM, Mohrig, D, Hajek, EA, and Heller, PL 2014. Paleoslope reconstruction in sand suspended-load dominant rivers. *Journal of Sedimentary Research* 84, 825–836.

Malin, MC and Edgett, KS 2000. Sedimentary rocks on early Mars. *Science* 290, 1927–1937. DOI:10.1126/science.290.5498.1927.

Malin, MC and Edgett, KS 2003. Evidence for persistent flow and aqueous sedimentation on early Mars. *Science* 302, 1931–1934. http://dx.doi.org/10.1126/science.1090544

Mangold, N, Kite, ES, Kleinhans, MG *et al.* 2012. The origin and timing of fluvial activity at Eberswalde Crater, Mars. *Icarus* 220, 530–551. http://dx.doi.org/10.1016/j.icarus.2012.05.026

Montgomery, DR and Buffington, JM 1997. Channel-reach morphology in mountain drainage basins. *GSA Bulletin* 109(5), 596–611.

Moore, JM and Howard, AD 2005. Large alluvial fans on Mars. *Journal of Geophysical Research* 110(E4), E04005. DOI:10.1029/2004JE002352.

Moore, JM, Howard, AD, Dietrich, WE, and Schenk, PM 2003. Martian layered fluvial deposits: implications for Noachian climate scenarios. *Geophys. Res. Lett.* 30(24), http://dx.doi.org/10.1029/2003GL019002.

Morgan, AM, Howard, AD, Hobley, DE *et al.* 2014. Sedimentology and climatic environment of alluvial fans in the Martian Saheki crater and a comparison with terrestrial fans in the Atacama Desert. *Icarus* 229, 131–156.

Palucis, MC, Dietrich, WE, Hayes, A *et al.* 2014. The origin and evolution of the Peace Vallis fan system that drains to the Curiosity landing area, Gale Crater, *Mars. J. Geophys. Res. Planets* 119, 705–728. DOI:10.1002/2013JE004583.

Paola, C and Mohrig, D 1996. Palaeohydraulics revisited: Paleoslope estimation in coarse-grained braided rivers. *Basin Res.* 8, 243–254.

Parker, G 1978. Self formed rivers with stable banks and mobile bed: Part II, the gravel river. *J. Fluid Mech.* 89(1), 27–148.

Parker, G 2008. Transport of gravel and sediment mixtures. In *Sedimentation Engineering: Processes, Measurements, Modeling, and Practice*, Vol. 110 (ed. MH García). American Society of Civil Engineers: Reston, VA; 165–252.

Parker, G, Wilcock, PR, Paola, C *et al.* 2007. Physical basis for quasi-universal relations describing bankfull hydraulic geometry of single-thread gravel bed rivers. *J. Geophys. Res. Earth Surface* 112(F4). DOI: 10.1029/2006JF000549.

Pepin, E, Carretier, S, Guyot, JL, and Escobar, F 2010. Specific suspended sediment yields of the Andean rivers of Chile and their relationships to climate, slope, and vegetation. *Hydrol. Sci. J.* 55(7), 1190–1205. DOI:10.1080/02626667.2010.512868

Pondrelli, M, Rossi, AP, Marinangeli, L *et al.* 2008. Evolution and depositional environments of the Eberswalde fan delta, Mars. *Icarus* 197, 429–451. 10.1016/j.icarus.2008.05.018

Prancevic, JP, Lamb, MP, and Fuller, BM 2014. Incipient sediment motion across the river to debris-flow transition. *Geology* 42(3), 191–194.

Rice, MS, Bell III, J, Gupta, S *et al.* 2013. A detailed geologic characterization of Eberswalde crater, Mars. *Mars* 8, 15–59. http://dx.doi.org/10.1555/mars.2013.0002

Ryan, SE, Porth, LS, and Troendle, A 2005. Coarse sediment transport in mountain streams in Colorado and Wyoming, USA. *Earth Surface Processes and Landforms* 30(3), 269–288. DOI:10.1002/esp.1128.

Seizilles, G, Devauchelle, O, Lajeunesse, E, and Metivier, FM 2013. Width of laminar laboratory rivers. *Physical Review E* 87, 05224.

Stock, JD 2013. Waters divided: a history of alluvial fan research and a view of its future. In *Treatise on Geomorphology*, Vol. 9 (ed J. Shroder and E. Wohl). Elsevier: Amsterdam; 413–458.

Syvitski, JPM, Peckham, SD, Hilberman, R, and Mulder, T 2003. Predicting the terrestrial flux of sediment to the global ocean: a planetary perspective. *Sediment. Geol.* 162(1–2), 5–24.

Thomson, BJ, Bridges, NT, Milliken, R *et al.* 2011. Constraints on the origin and evolution of the layered mound in Gale Crater, Mars using Mars Reconnaissance Orbiter data. *Icarus* 214(2), 413–432. DOI: 10.1016/j.icarus.2011.05.002.

Trampush, SM, Huzurbazar, S, and McElroy, B 2014. Empirical assessment of theory for bankfull characteristics of alluvial channels. *Water Resour. Res.* 50, 9211–9220. DOI:10.1002/2014WR015597.

Venditti, JG and Church, M 2014. Morphology and controls on the position of a gravel-sand transition: Fraser River, *British Columbia. J. Geophys. Res. Earth Surf.* 119, 1959–1976. DOI:10.1002/2014JF003147.

Wohl, E and Merritt D 2005. Prediction of mountain stream morphology. *Water Resources Research* 41, W08419. DOI:10.1029/2004WR003779.

Williams, RME, Irwin III, RP, and Zimbelman, JR 2009. Evaluation of paleohydrologic models for terrestrial inverted channels: Implications for application to martian sinuous ridges. *Geomorphology* 107, 300–315.

Williams, RME, Grotzinger, JP, Dietrich, WE *et al.* 2013. Martian fluvial conglomerates at Gale crater. *Science* 340, 1068–1072. DOI:10.1126/science.1237317.

Wilson, L, Ghatan, G, Head, J, and Mitchell, K 2004. Mars outflow channels: a reappraisal of the estimation of water flow velocities from water depths, regional slopes, and channel floor properties. *J. Geophys. Res.* 109, E09003.

Wood, LJ 2006. Quantitative geomorphology of the Mars Eberswalde delta. *Geol. Soc. Am. Bull*, 118(5–6), 557–566, http://dx.doi.org/10.1130/B25822.1.

Woodsworth, R, Forget, F, Millour, E *et al.* 2013. Global modeling of the early Martian climate under a denser $CO_2$ atmosphere: Water cycle and ice evolution. *Icarus* 222(1), 1–19. DOI:10.1016/j.icarus.2012.09.036.

Yingst, RA, Kah, LC, Palucis, MC, Williams *et al.* 2013. Characteristics of pebble and cobble-sized clasts along the Curiosity rover traverse from Bradbury Landing to Rocknest. *J. Geophys. Res. Planets* 118(11), 2361–2380. DOI:10.1002/2013JE004435.

## Discussion

### Discussion by Colin Thorne and Mike Miles

The authors note that, "*A simple power law between channel width and discharge (derived from terrestrial rivers) may provide a more accurate estimate of discharge than mechanistic approaches.*" We agree. Hydraulic geometry equations predict width as a function of discharge and for application to Martian streams, the authors correctly reverse the dependence of the variables in deriving their regression equation (Williams 1983). This approach was pioneered in the UK during the 1980s (Wharton *et al.* 1989), and subsequently published as the "Channel-geometry Method" (Wharton 1995).

The coefficients in the best-fit regression equations for the two analyses are identical; the exponents differ. In most *hydraulic geometry* equations, the exponent is not significantly different from 0.5 (Soar and Thorne 2000), suggesting an exponent close to two in a power relationship for $Q$ as a function of $w$. This is very close to Wharton's exponent (1.97). We would value the authors' interpretation of likely reasons for the lower exponent in their best-fit equation, which appears from Figure 28.10 to be due to inclusion of width data for large rivers with widths one or two orders of magnitude larger than those in Wharton's data set. We also suggest that adding confidence intervals to the graph in Figure 28.10 might add value by illustrating the degree of uncertainty in single and mean responses and would welcome the authors' view on this.

## References

Soar, PJ and Thorne, CR 2001. *Channel Restoration Design for Meandering Rivers.* Final Report ERDC/CHL CR-01-1, US Army Research and Development Center: Vicksburg; 416 pp. plus appendices. http://libweb.wes.army.mil/uhtbin/cgisirsi/2fD4nuOSuv/ERDC_VBG/185360025/523/6327

Wharton, G 1995. The channel-geometry method: guidelines and applications. *Earth Surface Processes and Landforms* 20(7), 649–660.

Wharton, G, Arnell, NW, Gregory, KJ, and Gurnell AM. 1989. River discharge estimated from channel dimensions. *Journal of Hydrology* 106(3), 365–376.

Williams, GP 1983. Palaeohydrological methods and some examples from Swedish fluvial-environments. *I. Cobble and boulder deposits. Geografiska Annaler Series A* 65(3–4), 227–243.

**Discussion by Jonathan Laronne**

A variety of evidence has been available during the past decade that water was available on Mars, with even more convincing confirmation from the very recent months that at select locations it presently runs on the surface. Your paper is also based on several types of evidence, the most crucial is one of relatively close-up and very interesting photographs (Figures 28.2a–d) of a rock formation that has an obvious granular makeup and an appearance of a clastic deposit. In this photograph the particles are only slightly rounded, hence restating your words, if a meander is a meander, is this sufficiently convincing to ensure that it is fluvial gravel?

**Discussion by Gordon Grant**

Have you looked at the Froude numbers for your Martian rivers, not in a deterministic way, but as a check on your flow estimates? I would be suspicious, for example, if your results suggested supercritical flow where your channel dimensions are at least reasonably constrained.

**Discussion by Mike Miles and Colin Thorne**

Chinn and Mason (2015) summarize long-term hydrology data for the Onyx River, Antarctica – see our discussion of Session 16, Shaw and Healy (1980), and Head and Marchant (2014). Our analysis of these data indicates the 2-year return period daily and instantaneous flows (taken as representing bankfull discharge) are 2 and 3 $m^3/s$, respectively. Measurements on GoogleEarth indicate bankfull widths (in single-thread reaches) varying between 6 and 13 m. Figure 28.10 suggests that bankfull discharge in the Onyx River should be larger, ranging between 4 and 14 $m^3/s$. As Antarctic stream banks lack vegetation, which is known to result in wider channels when other bank properties are held constant, this is not unexpected.

This cursory analysis suggests that the hydraulic geometry relationships for unvegetated, high-latitude streams should be further investigated as possible analogues for ancient Martian streams and the effects of ice-rich permafrost on streambank stability (Church and Miles, 1982) and channel geometry should be better defined. Perhaps we should arrange a joint field trip to some polar streams (though probably on Earth rather than Mars!)?

## References

Chinn, T and Mason, P 2015. The first 25 years of the hydrology of the Onyx River, Dry Valleys, Antarctica. *Polar Record* 52(1), 16–65. DOI:10.1017/S0032247415000212.

Church, MA and Miles, MJ 1982. Processes and mechanisms of riverbank erosion – discussion. In *Engineering Problems in the Management of Gravel-Bed Rivers* (ed. RE Hey). John Wiley & Sons: Chichester, UK; 259–268.

Head, JW and Marchant, DR 2014. The climate history of early Mars: insights from the Antarctic McMurdo Dry Valleys hydrologic system. *Antarctic Science* 26(6), 774–800.

Shaw, J and Healy, TR 1980. Morphology of the Onyx River system, McMurdo Sound region, Antarctica. *New Zealand Journal of Geology and Geophysics* 23(2), 223–238.

**Discussion by John Buffington**

Hydraulic geometry offers robust scaling of channels across many orders of magnitude in natural rivers, irrigation canals, and laboratory channels (Ferguson 1986). Although the authors' analysis focuses

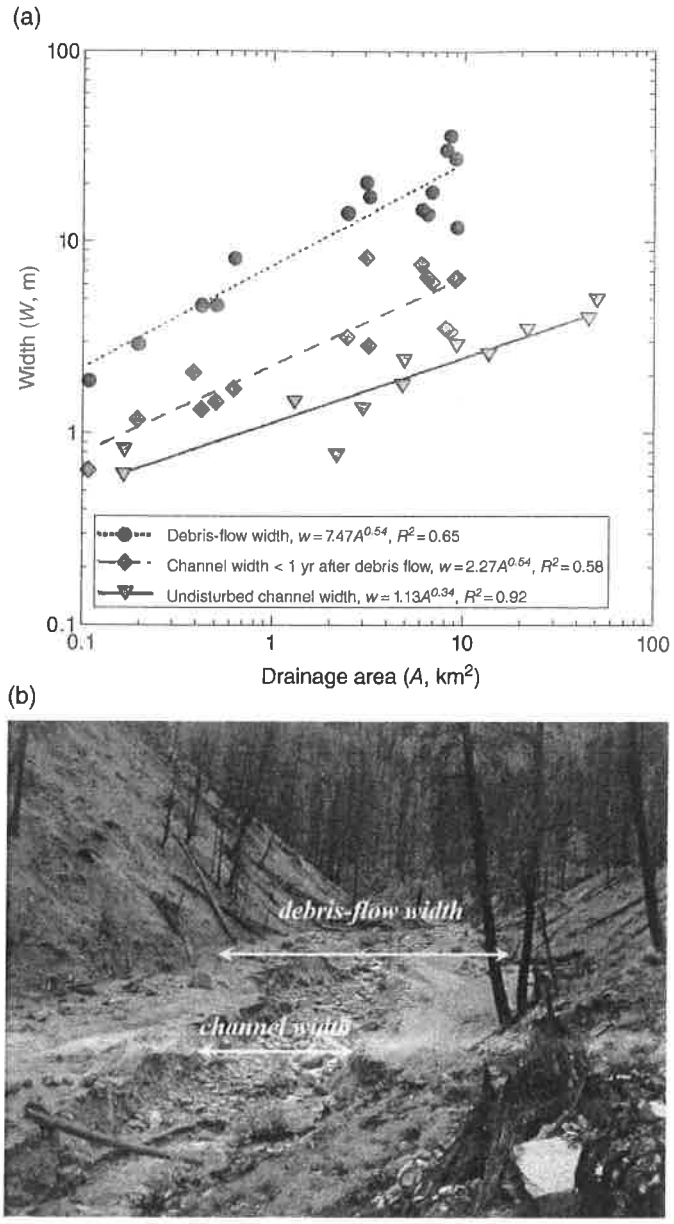


**Figure 28.15** (a) Width as a function of drainage area for (i) post-fire debris flows (circles), (ii) channels carved into the debris-flow deposits via a mixture of hyperconcentrated and fluvial flows within the first year following disturbance (diamonds), and (iii) undisturbed fluvial channels in neighboring basins (inverted triangles). The study sites are mountain streams in confined, alluvial valleys (plane-bed, step-pool, and cascade morphologies, with gravel to boulder beds, and channel slopes > 1%) in the upper Boise River, central Idaho, USA. Debris flows were triggered by intense thunderstorms on bare, hydrophobic soils following fire. Subsequent thunderstorm and snowmelt runoff incised channels into the debris-flow deposits via hyperconcentrated and fluvial flows for bare, unvegetated banks. Undisturbed channels are produced by predominantly snowmelt runoff, with banks well-vegetated by shrubs and conifers, resulting in smaller channel widths for a given drainage area. (b) Photograph illustrating debris-flow width and width of channel subsequently carved into the debris-flow deposit.

on fluvial deposits, it is worth noting that hydraulic geometry relations can be developed for a variety of fluids, which may have relevance for some Martian channels given that differences in gravity and atmospheric conditions (pressure, temperature, and, thus, viscosity) may cause channel hydraulics and flow rheology (Froude and Reynolds numbers) to differ from those on Earth. Data from mountain rivers in Idaho provide an example of how channel width responds to differences in erosional processes, flow rheology, runoff characteristics, and degree of riparian vegetation within a given physiographic region (similar topography, geology, and climate) following fire disturbance (Figure 28.15). In all cases, the exponent of the hydraulic geometry equation is within the range typically observed for terrestrial alluvial and bedrock rivers (0.3–0.6; Montgomery and Gran 2001; Wohl 2004) but systematic differences in width are evident. The debris-flow widths are event-based responses and the post-debris-flow channel widths are transient responses following disturbance, both of which differ from the long-term bankfull conditions examined by the authors, but they nonetheless provide some sense of scaling for different formative processes across a range of rheological and environmental conditions.

## References

Ferguson, RI 1986. Hydraulics and hydraulic geometry. *Progress in Physical Geography*, 10(1), 1–31.

Montgomery, DR and Gran KB 2001. Downstream variations in the width of bedrock channels. *Water Resources Research* 37(6), 1841–1846.

Wohl, E 2004. Limits of downstream hydraulic geometry. *Geology* 32(10), 897–900.

### Reply by the Authors

The discussions touch on three important issues in the paper. (i) Are gravel deposits observed during the *Curiosity* mission convincingly of fluvial origin? (ii) Are the derived hydraulic expressions sensible, and, specifically, do they predict flows to be subcritical rather than supercritical in most circumstances? (iii) What is the significance of the specific power law relationship of bankfull discharge versus bankfull width (Equation (28.21)) and what processes might influence the relationship on Mars?

Jonathan Laronne comments that the gravels visible in our figures appear to be only slightly rounded and might this challenge the interpretation of their fluvial origin. For the outcrops shown in Figure 28.2 (and a nearby exposure), Williams *et al.* (2014) measured 535 gravels and concluded that the majority of the pebbles are subrounded to rounded (based on the qualitative Powers' roundness indices). Yingst *et al.* (2013) demonstrated that roundness measured at the outcrops shown in our Figure 28.2 was much greater than that found in previous missions on Mars. Williams *et al.* (2014) suggested the rounding required a minimum of several kilometers of transport, but was likely more given the reduced abrasion rates of less intense collisions of bedload transport on Mars. Szabo *et al.* (2015) employ other measures to document rounding of gravels observed by the *Curiosity* rover and conclude that rounding due to fluvial transport likely developed over distances of tens of kilometers by fluvial processes. Grotzinger *et al.* (2015) provide outcrop description, placing conglomerates in a fluvial deltaic system propagating from Gale Crater wall towards the center of the crater. Collectively these analyses argue strongly that these are fluvially transported gravels.

Gordon Grant suggests we review the Froude number implications of our derived hydraulic relationships, with the expectation that if the calculations predict falsely supercritical conditions it should be a concern. We calculated the Froude number by using Equations (28.12) and (28.8) (which are based on a threshold shear stress concept) and compared that to the Froude number $Fr$ calculated

from the observed bankfull velocity and depth values reported in Li *et al.* (2014). The regression yielded $Fr_{observed} = 0.97\ Fr_{predicted} + 0.02$, so a close comparison, but with considerable variance yielding only an $R^2$ of 0.38. None of the predictions exceeded a *Fr* number of 1.0 and only four of the observed values did. The *Fr* values calculated from Equations (28.17) and (28.15), expressions that use an empirical relationship for the bankfull shear velocity, showed essentially no correlation with observed *Fr* and predicted 24 of the rivers would have supercritical flows at bankfull. Hence, the performance is poorer but does not excessively overpredict supercritical conditions. The *Fr* derived from Equations (28.12) and (28.8) is independent of gravity (the gravity term in the velocity expression cancels the gravity term in the *Fr*) and thus the incidence of supercritical flow is not expected to be higher on Mars. The *Fr* derived from the empirical shear velocity relationship indicates that *Fr* is also only weakly dependent on gravity.

Colin Thorne and Mike Miles ask why the exponent in the plot of bankfull discharge versus bankfull width is not closer to the inverse of the common exponent of 0.5 when width is plotted against discharge. The least squares approach used in regressions typically leads to exponents that are not the inverse of each other when the variables are reversed. Also, many have reported discharge–width relationships in regional surveys, and Wharton (1995) summarized findings in his table 1. His value of 1.97 for British rivers is an exception. For the nine large data sets from western US rivers used in analyses by Osterkamp and Hedman (1977; cited in Wharton 1995), the exponents for the nine studies ranged from 1.4 to 1.97, but with six lying between 1.60 and 1.71, i.e. very similar to values reported in Equations 28.19 through 28.21. Many factors influence channel width, which Osterkamp and Hedman (1997), for example, explicitly explore empirically, and as John Buffington illustrates in his discussion of this paper. Our approach was to combine two recent data summaries with additional data from sources not included in these two summaries that represented smaller, steeper, and coarser bedded rivers. The data are all based on field measurements, including bankfull discharge. The streambed material ranged from sand to boulders and we purposely sought a wide range of conditions given the large uncertainty of Martian conditions. The data field is biased towards US rivers and to channels between 2 and 100 m wide. The largest rivers are lowland tropical sand-bedded rivers. The slope of the correlation reported in Figure 28.10 with a 95% confidence interval is $1.66 \pm 0.04$. Note that for the largest channel widths the data density is smaller and the range about the regression is about a factor of two. For the high data density the range about the regression is about 10. The width range for a given discharge is much less. The data from small Antarctic streams reported by Miles and Thorne fall within the data field shown in Figure 28.10. The range of variance of data, assuming measurements are accurate, reflect the varying factors that influence channel width for a given discharge, e.g., bank strength, sediment supply, bed grain size, flow dynamics, and process dominance. A conservative application of Equation 28.21 to Mars would be to assume that for a given calculated discharge the range could be a factor of ten larger or smaller. Despite this large uncertainty, such data provide key hydroclimatological information of the history of Mars.

## Reference

Szabo, T, Domokos, G, Grotzinger, JP, and Jerolmack, DJ 2015. Reconstructing the transport history of pebbles on Mars. *Nature Communications* 6, 8366. DOI:10.1038/ncomms9366.